Photo-Fenton Treatment of a Pharmaceutical Industrial Effluent Under Safe pH Conditions

Reyna Natividad, Arisbeth Mendoza, Sharon E. Brewer,
Sandra Luz Martínez-Vargas, J. L. Pérez-Mazariego,
Karen Adriana Novoa, Leobardo Manuel Gómez-Oliván, and Rubi Romero

Contents

R. Natividad, A. Mendoza, and R. Romero (✉)
Chemical Engineering Lab., Centro Conjunto de Investigación en Química Sustentable,
UAEM-UNAM, Universidad Autónoma del Estado de México, Toluca, Mexico
e-mail: rromeror@uaemex.mx

S. E. Brewer
Chemistry Department, Faculty of Science, Thompson Rivers University, Kamloops, BC,
Canada

S. L. Martínez-Vargas, K. A. Novoa, and L. M. Gómez-Oliván
Faculty of Chemistry, Universidad Autonoma del Estado de México, Paseo Colón Esq. Paseo
Tollocan, Toluca, Mexico

J. L. Pérez-Mazariego
Physics Department, Faculty of Science, Universidad Nacional Autonoma de Mexico, Ciudad
de México, Mexico

Abstract This chapter aims to present the effect of treating a pharmaceutical industrial effluent by photo-Fenton catalyzed with a Fe-pillared bentonite. XRD proved the pillaring process successful, and by N_2 physisorption, it was established that the specific surface area of bentonite (34 m^2/g) increased to 277 m^2/g and pore volume increased from 0.058 to 0.106 cm^3/g. Active Fe species were identified by Mössbauer spectroscopy. The effect of reaction variables such as catalyst loading, pH, H_2O_2 concentration, and initial concentration of total organic carbon (TOC) is also presented. It was concluded that to reach near 100% mineralization, an acidic pH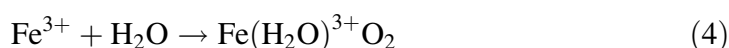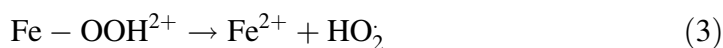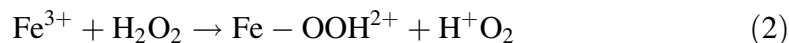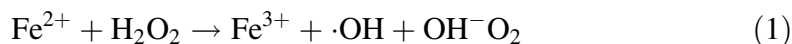 (2.7) should be observed. A high mineralization under these conditions, however, does not directly correlate with a low toxicity. Actually, the oxidative stress biomarkers only decreased when pH was not modified (pH = 8) albeit the attained mineralization was only 51%. It is worth noticing that the use of pillared clays allows carrying out photo-Fenton treatment under pH conditions other than acidic. The synthesized catalyst exhibited magnetism and this can be used for an easier recovery.

Keywords AOPs, Emerging contaminants, Mineralization, Photocatalysis, Toxicity, Wastewater

1   Introduction

The pharmaceutical production is one of the biggest problems related to water pollution. In Mexico, it has been shown that pharmaceutical industry effluents are a mixture of a variety of compounds frequently toxic [1], which include excipients, pharmaceutical drugs, and washing products. In this context, the effluents of production processes of emerging contaminants, such as nonsteroidal anti-inflammatory drugs (NSAIDs), are receiving special attention. Among NSAIDs, paracetamol or acetaminophen stands out because worldwide it is highly consumed and therefore highly produced. The importance of effective treatment of paracetamol containing effluents is related to toxicological effects in aquatic environment [2], since the degradation products of paracetamol are potentially toxic, causing on indicator species oxidative stress and cellular damage or death and inhibition of reproduction [3]. This has motivated the study and development of processes that contribute to the treatment of theses pollutants. Particularly attractive options are the advanced oxidation processes (AOPs). Among these, there are the well-known Fenton and photo-Fenton processes. The Fenton process involves the reaction of Fe(II) with H_2O_2 to produce hydroxyl radicals (HO$^{\cdot}$) via reaction 1. Under suitable conditions, the process is considered catalytic due to the reduction of Fe(III) by reactions 2 and

3. Yet with this, the regeneration of Fe(II) is not efficient enough, and sludge is generated by precipitation of species of Fe(III). Although this sludge can contribute to the removal of organic matter, it is desirable to degrade it and not only change its phase. In order to reduce this problem and increase the efficiency of this process, UV radiation is added. By this means, more hydroxyl radicals are produced by photoreducing Fe(III) to Fe(II) (reactions 4–6), and this process is called photo-Fenton [4–6].

$$Fe^{2+} + H_2O_2 \rightarrow Fe^{3+} + \cdot OH + OH^- O_2 \tag{1}$$

$$Fe^{3+} + H_2O_2 \rightarrow Fe - OOH^{2+} + H^+ O_2 \tag{2}$$

$$Fe - OOH^{2+} \rightarrow Fe^{2+} + HO_2 \tag{3}$$

$$Fe^{3+} + H_2O \rightarrow Fe(H_2O)^{3+} O_2 \tag{4}$$

$$Fe(H_2O)^{3+} \rightarrow Fe(OH)^{2+} + H^+ \tag{5}$$

$$Fe(OH)^{2+} + h\nu \rightarrow Fe^{2+} + OH \tag{6}$$
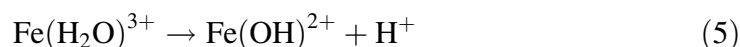
Importantly, in this process, it is necessary to control the pH of the medium because the Fenton and photo-Fenton reactions exhibit high activity at pH about 2.8 [7]; at pH greater than 3.0, the reaction is slower because the generation of insoluble iron hydroxides decreases the concentration of the Fe(III) ion in solution and thus radiation transmission [8]. In spite of its high efficiency [9, 10], some undesirable features of the homogeneous photo-Fenton process are high hydrogen peroxide consumption, radiation field diminishment, the need of a separation step to remove the added iron, and the addition of chemicals to maintain an acidic pH for iron ions to be in solution [5]. These disadvantages have led to the investigation of solid supports capable of maintaining iron immobilized. In this sense, recent studies have shown that bentonite clay promises to be good catalyst support by modifying its surface [11, 12]. Among the different ways of modifying bentonite, the pillaring has been considered as a good alternative since the resulting material exhibits a high catalytic activity for removal of organic contaminants, stability against pH changes in the solution, high specific surface area, and relatively easy separation from treated effluents [11].

Herein, the toxicity reduction of a pharmaceutical industry effluent treated by photo-Fenton process catalyzed with an iron-pillared clay (Fe-PILC) is described. The synthesis of this catalyst as well as its characterization and mineralization results is also included.

2   Photo-Fenton Catalyst

2.1   Fe-PILC Synthesis

The catalyst used to conduct the study described here was an iron-pillared clay (Fe-PILC), and it was prepared by the method reported by Martin del Campo and Valverde [11, 13] as follows: 300 mL $FeCl_3 \cdot 6H_2O$ (aqueous solution 0.2 M) was slowly added to 600 mL of NaOH aqueous solution 0.2 M at room temperature under continuous stirring. The so obtained mixture was stirred for 4 h at room temperature and pH between 1.78 and 1.8 using hydrochloric acid 5 M. These pH values are important in order to generate the corresponding iron hydroxides in solution. The pillaring solution was slowly added to the 0.1 wt% aqueous bentonite suspension under stirring. The next step was to recover the clay by centrifugation and washed with distilled and deionized water in order to remove the chlorides. The product was dried overnight at 75°C and calcined for 2 h at 400°C. For this synthesis, the following reagents were employed sodium hydroxide (NaOH), ferric chloride hexahydrate ($FeCl_3 \cdot 6H_2O$ with purity of 99%), and hydrochloric acid (37%). Moreover, deionized and distilled water were provided by HYCEL and bentonite (pure grade) supplied by Thermo Fisher Scientific. This clay has a particle size >2 μm and a cation exchange capacity of 94 meq/100 g.

2.2   Fe-PILC Characterization

Figure 1 is the diffractogram of iron-pillared clay (Fe-PILC). This XRD pattern was obtained by a Bruker Advance 8 instrument using *Cu-Kα* radiation at 35 kV and 30 mA and was collected from 0 to 40° (2θ) with a step of 0.04°/min. At 4° (2θ), a small reflection that is commonly associated with pillaring processes can be observed [11, 14]. Three reflections of interest are observed, the first at 20° corresponding to (FeO(OH)), the other two at 26 and 35 related to hematite (Fe_2O_3) [15].

Figure 2 shows the room temperature Mössbauer spectrum of pure bentonite, and it was fitted with two doublets. One doublet with isomer shift $\delta = 0.32$ mm/s and a quadrupole splitting $\Delta Q = 0.44$ mm/s corresponding to Fe^{3+} in octahedral site and the other one with $\delta = 1.02$ mm/s and $\Delta Q = 2.95$ mm/s corresponding to Fe^{2+} [16–19]. The ratio Fe^{2+}/Fe^{3+} in this bentonite is unusually high.

Figure 3 shows the Mössbauer spectrum of Fe-PILC at room temperature. We can see that there is no contribution of Fe^{2+} to the signal probably because Fe^{2+} ions migrated to Fe^{3+} into the pillared clay layers [20, 21] or because Fe^{2+} stabilizes the formation of Fe_3O_4. The Fe-PILC Mössbauer data was fitted with three doublets, one of them corresponding to Fe^{3+} in octahedral site of bentonite with $\delta = 0.36$ mm/s and $\Delta Q = 0.43$ mm/s, another with $\delta = 0.36$ mm/s and $\Delta Q = 0.69$ mm/s corresponding to Fe^{3+} in γ-FeOOH [22–24], and the doublet with the major contribution, with
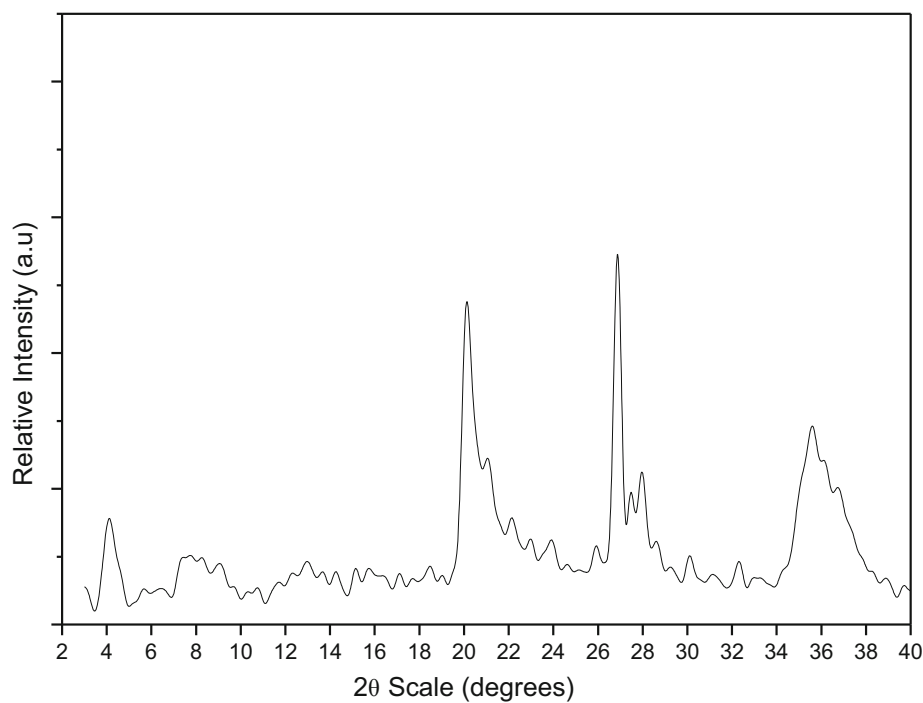
Fig 1 X-ray diffractogram of Fe-PILC
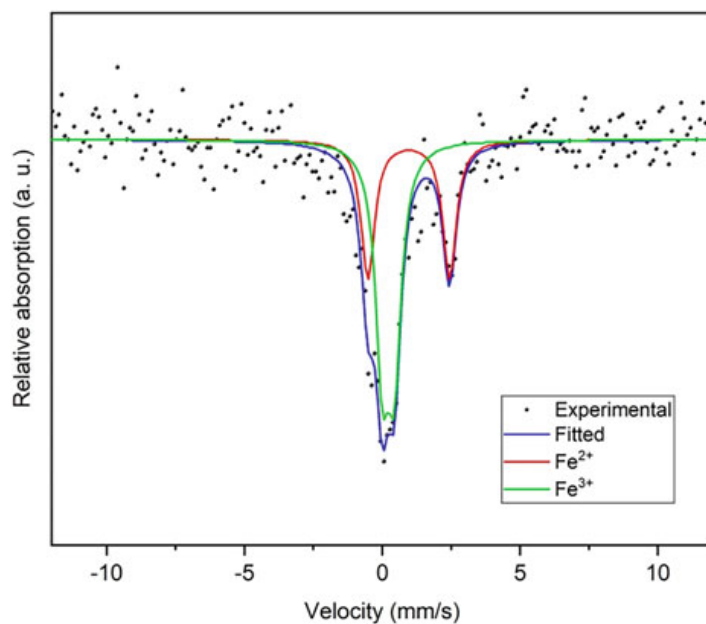
Fig 2 Mössbauer spectrum of bentonite

$\delta = 0.329$ mm/s, $\Delta Q = 0.88$ mm/s assigned to nanoparticles of magnetite (Fe_3O_4) [25–27]. The doublet associated to Fe_3O_4 has a FWHM $= 0.71$ mm/s suggesting that there is a size distribution of magnetite nanoparticles in Fe-PILC and probably this oxide is forming the pillars [20]. The presence of lepidocrocite (γ-FeOOH) in Fe-PILC is not a surprise since there are reports indicating that lepidocrocite is an intermediate product in the magnetite synthesis [28–30]. Table 1 shows the

Fig. 3 Mössbauer spectrum of Fe-PILC at room temperature

Table 1 Mössbauer parameters of pure bentonite and Fe-PILC at room temperature

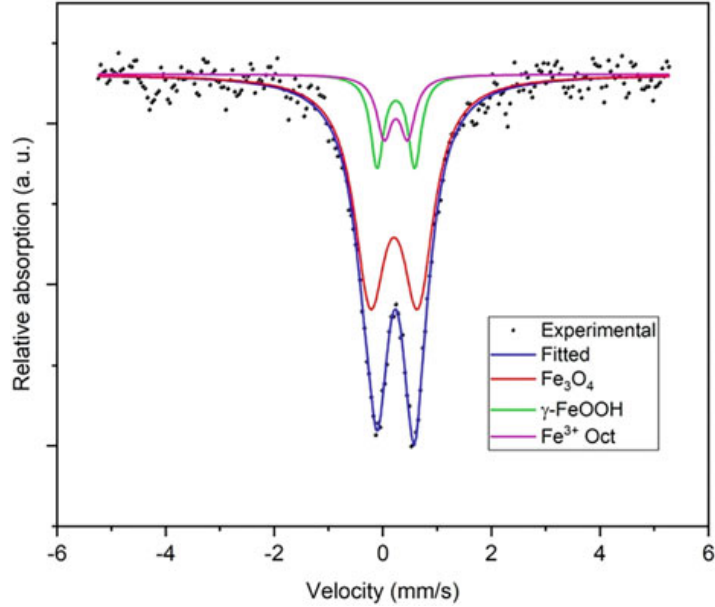| Site	δ (mm/s)	ΔQ (mm/s)	Γ (mm/s)	%
Bentonite				
Fe^{3+}	0.340 ± 0.072	0.44 ± 0.01	0.6[a]	60.0 ± 0.8
Fe^{2+}	1.079 ± 0.094	2.96 ± 0.02	0.6[a]	40.0 ± 1.0
Fe-PILC				
Fe_3O_4	0.329 ± 0.030	0.88 ± 0.03	0.710 ± 0.072	76.0 ± 0.5
γ-FeOOH	0.362 ± 0.037	0.69 ± 0.01	0.28 ± 0.02	14.0 ± 0.2
Fe^{3+} Oct	0.363 ± 0.052	0.43 ± 0.02	0.34 ± 0.02	10.0 ± 0.3

δ is the isomer shift respect to metallic iron, ΔQ the quadrupole splitting, and Γ the FWHM
[a]Fixed

Mössbauer parameters of pure bentonite and Fe-PILC at room temperature. It is important to mention that the powder of Fe-PILC is attracted by a magnet confirming the presence of magnetite, and this is in agreement with XPS results [31].

Regarding textural properties, the clay pillaring process implies an increase in specific surface area and pore volume. The specific surface area of bentonite (34 m^2/g) increases to 277 m^2/g, and pore volume increases from 0.058 to 0.106 cm^3/g. This is attributed to the formation of iron oxides between clay layers [32]. For N_2 physisorption studies, a Quantachrome Autosorb analyzer was used with N_2 adsorption relative pressure $P/P_o = 0.99$ and 77°K, and degassing condition clay were achieved at 250°C for 2 h under vacuum of 6.6×10^{-9} bar. The specific surface area was calculated according to Brunauer-Emmett-Teller method (BET). The iron content of the Fe-PILC used in this work was 17%, and this was established by atomic absorption using an AA240FS VARIAN spectrometer with a calibration curve of a standard solution of Fe.

3   Effluent Characterization

The treated effluent was obtained from an NSAID-manufacturing plant in Lerma (State of Mexico) and was sampled according to the official Mexican norm for wastewater sampling (NMX-AA-003-1980). Sampling point was in the production area that connects directly to the municipal sewer. The following physicochemical characteristics of the effluent were determined: total organic carbon (TOC) with a Shimadzu TOC analyzer, TOC-L CPN with integrated autosampler Shimadzu ASI-L, chemical oxygen demand (COD) according to the NMX-AA-030-SCFI-2001 using a HACH DR/5000 and a digestive solution HACH, total suspended solids (TSS) and temperature according to NMX-AA-034-SCFI-2001 and NMX-AA-007-SCFI-2013 norms, and turbidity and dye with the NMX-AA-0038-SCFI-2001 and NMX-AA-45-SCFI-2001 methods in a HACH DR/4000. The quantification of paracetamol (PAR) in water was determined by the method reported by San Juan [33] using liquid chromatography tandem-mass spectrometry (LC-MS/MS) and employing an Agilent 1290 Infinity HPLC unit (Santa Clara CA) and an RRHD Plus C_{18} (2.1 × 50 mm, 1.8 μm) chromatography column.

The official Mexican norm responsible for regulating the discharge of wastewater to sewage systems (NOM-002-SEMARNAT-1996) establishes limits only for COD, TSS, and temperature, these being 500 mg/L for COD and 220 mg/L for TSS and temperature of 40°C. The lack of inclusion of more physicochemical characteristics has led to increase water pollution and therefore damage to aquatic systems. Turbidity, TOC, and COD are key to the efficiency of the effluent treatment with photo-Fenton, being turbidity a limitation in the use of light [34]. The photo-Fenton process is used with low values of TOC and COD. Therefore, it is important to mention that the effluent COD and TOC are very high in comparison with effluents studied by Klamerth and Michael [2, 35]. Actually, it is worth clarifying that the TOC values of the industrial effluent were so high that mineralization was not observed at all and therefore it was decided to test different dilution degrees. It was found that the minimum dilution degree to observe mineralization was 1:100. The characterization of such diluted effluent is shown in Table 2.

4   Effluent Treatment

The results presented here were obtained in a reaction system consisting of a Pyrex glass batch reactor with a volume of 100 mL (2.5 cm in diameter and 20 cm of height), equipped with a UVP Pen-Ray Lamp of mercury of 5.5 W UV light (UVP) placed inside at the center of reactor. This lamp emits primary energy at 254 nm with a typical intensity of 4,400 μW/cm^2 and uses a UVP Pen-Ray power supply of 115 V/60 Hz. Also, there was inside the reactor an electrode Boeco Germany BA 17 connected to a pH meter accumet XL15, Fisher Scientific. Stirring was conducted using a magnetic stirrer and temperature was kept constant with a water bath. The

Table 2 Effluent characterization prior treatment

| Parameters	
TOC (mg/L)	178.0 ± 0.14
COD (mg/L oxígeno)	181 ± 0.7
pH	7.95 ± 0.005
Conductivity (µS/cm)	192 ± 0.1
Temperature (°C)	20
Turbidity (NTU)	193.0 ± 0.7
Dye (mg/L (Pt-Co))	0.45 ± 0.007
Paracetamol concentration (mg/L)	1.7 ± 0.03
TSS (mg/L)	12

photoreactor was intermittently operated using a reaction volume of 30 mL of effluent to be treated, and the experiments were performed using the following methodology: Initially, the effluent was charged, and thereafter, the catalyst was added and then stirred. After the pH was measured and adjusted as required (2.7, 5, or 8), the UV lamp was turned on and finally H_2O_2 (30%) was added. The temperature (T) and stirring were kept constant at $30 \pm 2°C$ and 800 rpm. Samples taken at different reaction times were subjected to a separation process in a centrifuge BOECO M-240 to remove the Fe-PILC. Sulfuric acid (96.9%) and hydrogen peroxide (30%), both from Fermont, were used to conduct the photo-Fenton process.

The studied variables were (1) initial catalyst concentration, (2) pH, (3) initial concentration of H_2O_2, and (4) initial concentration of total organic carbon of effluent. Given the diversity of materials used for the cleaning of areas coupled with those used in the manufacturing process, it was decided to use as primary response variable the total organic carbon (TOC) content.

In order to make evident the effect of photo-Fenton, initially, the effluent was separately treated with hydrogen peroxide (H_2O_2), catalyst (Fe-PILCs), and UV light. Experiments combining all of them (photo-Fenton) were also carried out. Total organic carbon (TOC) was used as response variable. It is worth pointing out that the H_2O_2 stoichiometric amount used in all experiments was calculated based on the TOC content of the effluent [36]. Figure 3 shows that in terms of mineralization, the best treatment of the effluent is the photo-Fenton process, since it shows a significant difference regarding TOC values with the other essayed treatments after 3 hours of reaction. These results showed that the photo-Fenton process can be carried out without changing pH effluent. At the same conditions, however, and only decreasing pH to 2.7, a greater mineralization of 51.0% was attained. Therefore, the other variables were studied under a pH 2.7, and further below the results of a systematic study of pH are also presented.

The results shown in Fig. 4 allow to discard the adsorption of contaminants onto the catalytic surface. Furthermore, from Fig. 4, it can also be inferred that the hydroxyl radical generation by photolysis of hydrogen peroxide via reaction 7 [37] is rather slow.

Fig. 4 Effluent mineralization percentage (%) after each treatment. Experimental conditions: catalyst loading $= 0.6$g/L; temperature $= 30°$C; pH $= 8$; stirring speed $= 800$ rpm; reaction time $= 180$ min

$$H_2O_2 + h\nu \rightarrow 2HO^{\cdot}O_2 \tag{7}$$
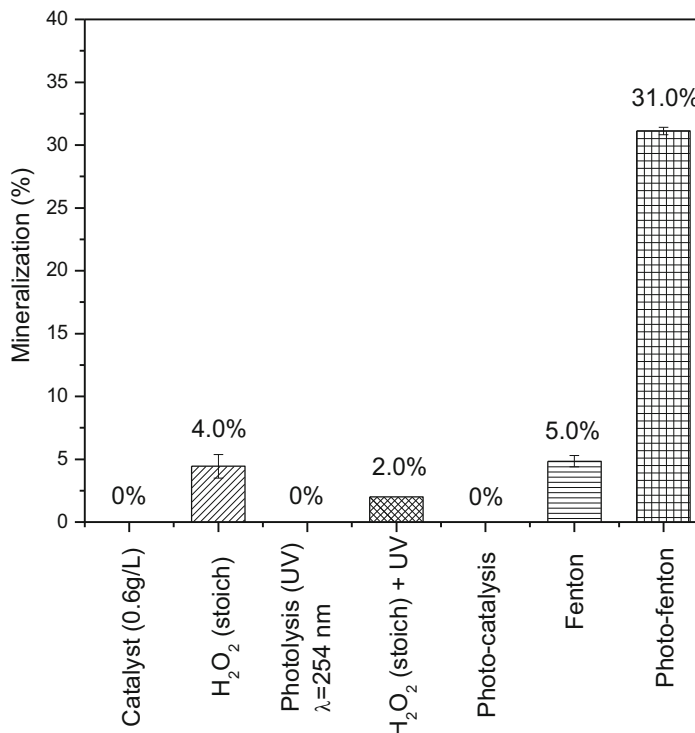
4.1 Effect of Catalyst Loading

The photo-Fenton process was performed with five different loadings of Fe-PILC, i.e., 0.4, 0.5, 0.6, 0.7, and 0.8 g Fe-PILC/L with a reaction time of 180 min. It can be observed in Fig. 5 that the smallest mineralization degree and rate were with a catalyst loading of 0.4 g/L. This can be ascribed to a low generation of hydroxyl radicals due to a small amount of Fe to catalyze hydrogen peroxide dissociation [38]. There were not significant differences with other catalyst loadings indicating that degradation exhibits the same oxidation resistance [39]. Still, if initial reaction rates are calculated (Fig. 5b), it can be observed that the best initial reaction rate is attained with a loading of 0.5 g/L and that initial reaction rate decreases after this catalyst dosage. This can be ascribed to an increase on turbidity that causes a reduction in UV light absorption, consequently decreasing the photoreduction of Fe(III) (reaction 6) [34, 40, 41]. The effect of this variable gives evidence that resistance to mass transfer from liquid to solid is negligible.

Fig. 5 (**a**) and (**b**) Effect of catalyst loading on TOC normalized content. Experimental conditions: temperature = 30°C; pH = 2.7; stirring speed = 800 rpm
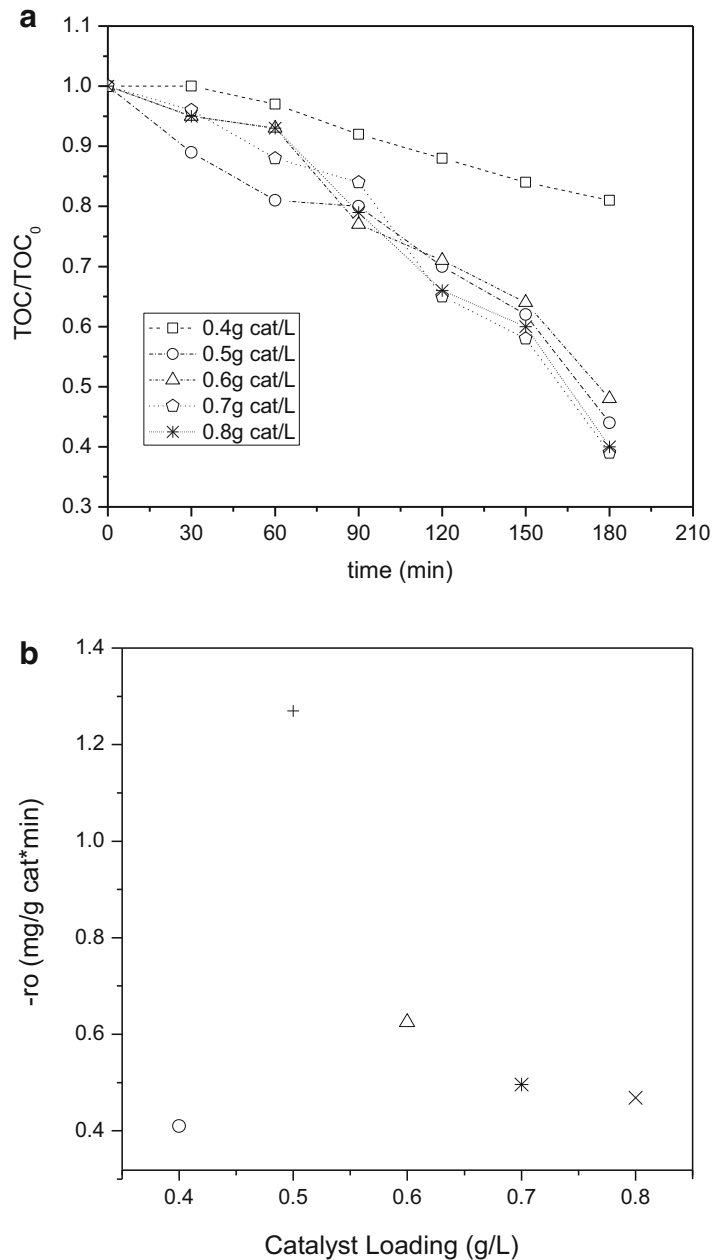
4.2 Effect of pH

A key variable to efficiently perform homogeneous Fenton and photo-Fenton processes is pH. This should be kept around 2.8 in order to minimize the formation of iron complexes. This pH value, however, is considered as a limiting factor [35, 42], and therefore, it is an important variable to be assessed in heterogeneous processes. This variable was studied in the photo-Fenton process at three values (2.7, 5.0, and 8.0). To achieve the acidic values, 0.1 M H_2SO_4 was added. The results plotted in Fig. 6 show that both mineralization degree and rate are significantly

Fig. 6 Effect of pH on normalized TOC profile. Reaction conditions: catalyst loading = 0.5g/L; temperature = 30°C; stirring speed = 800 rpm
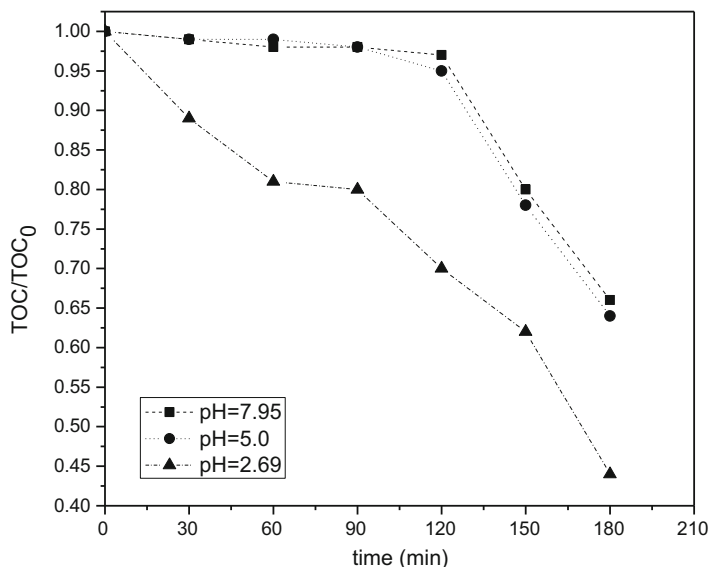
affected by pH. After 180 min of reaction, the mineralization percentages were 34, 32, and 56 at pH values 8, 5.0, and 2.7, respectively. The mineralization enhancement can be attributed to the iron oxides in the pillars of clay [43].

Iron leaching was quantified by atomic absorption and was found to be dependent on pH. At high pH, 5 and 8, an iron leaching of 1.3% was measured. At acidic pH, the iron leaching was greater than 4.4%. This suggests that the increase on mineralization rate can partially be ascribed to homogeneous photo-Fenton being promoted due to the higher leaching. Also, it is likely to be more rapid mineralization by reaction of iron oxides in the pillars with H^+ (reactions 8 and 9) increasing the production of radicals HO [44]. Despite pH 2.7 leading to a faster and higher mineralization, the photo-Fenton process without changing the pH of the effluent has the advantage of avoiding the use of additional reagents to neutralize the treated effluent.

$$2FeOOH + 4H^+ + H_2O_2 \leftrightarrow Fe^{2+} + O_2 + 4H_2O \tag{8}$$

$$Fe^{2+} + H_2O_2 \leftrightarrow Fe^{3+} + HO^\cdot + HO^-O_2 \tag{9}$$
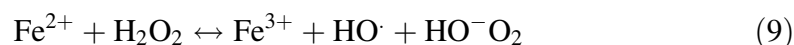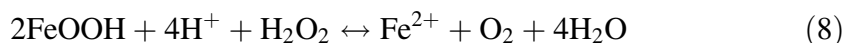
4.3 Effect of H_2O_2 Concentration

This variable was studied at three values (0.5∗stoich, stoichiometric, and 2∗stoich). The stoichiometric amount was calculated based on the TOC content of the effluent to be treated. In Fig. 7, it can be seen that the effluent mineralization was significantly affected by this variable. It can be observed that an H_2O_2 concentration above and below the stoichiometric one leads to a plateau after only 60 min of reaction. The

Fig. 7 Effect of H_2O_2 concentration on TOC normalized content. Experimental conditions: pH = 2.7; catalyst loading = 0.5 g/L; temperature = 30°C; stirring speed = 800 rpm
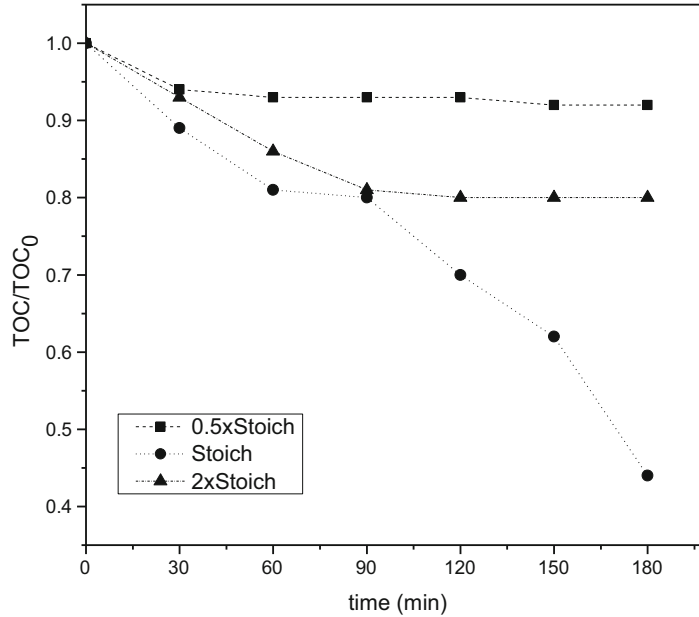

attained mineralization was 8% and 20%, with half and twice the stoichiometric amount of H_2O_2, respectively. The lowest achieved value (8%) can be attributed to the lack of H_2O_2 that limits the hydroxyl radical concentration and therefore is insufficient to react with organic molecules [45]. It was expected that increasing the concentration of H_2O_2 favored effluent mineralization due to the relationship with production of HO˙ radicals. This was not observed though. An excess of H_2O_2 probably caused a scavenging of HO radicals by reactions 10, 11, and 12 [12, 40, 46]. The best results were obtained by using the stoichiometric H_2O_2 amount, and an increase on the initial rate and mineralization percentage (56%) after 180 min of reaction was observed.

$$H_2O_2 + HO\cdot \rightarrow HO_2^- + H_2OO_2 \qquad (10)$$

$$HO_2^- + HO\cdot \rightarrow H_2O + O_2O_2 \qquad (11)$$

$$HO\cdot + HO\cdot \rightarrow H_2O_2 \qquad (12)$$
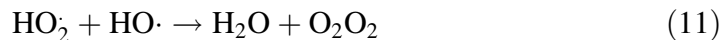
4.4 Effect of TOC Initial Concentration

The effect of TOC initial content is shown in Fig. 8. The experiments were performed with the following contents: 59, 95, and 178 mg/L with 0.5 g/L Fe-PILCs, stoichiometric concentration of hydrogen peroxide from 178 mg/L TOC, and pH between 2.65 and 2.69. It can be seen that the percentage of mineralization increases from 56% to 91% when decreasing the TOC content from 178 to 95 mg/L. Moreover, the maximum effluent mineralization percentage is not affected

Fig. 8 Effect of initial TOC on mineralization extent. Experimental conditions: pH = 2.7; catalyst loading = 0.5 g/L; temperature = 30°C; stirring speed = 800 rpm
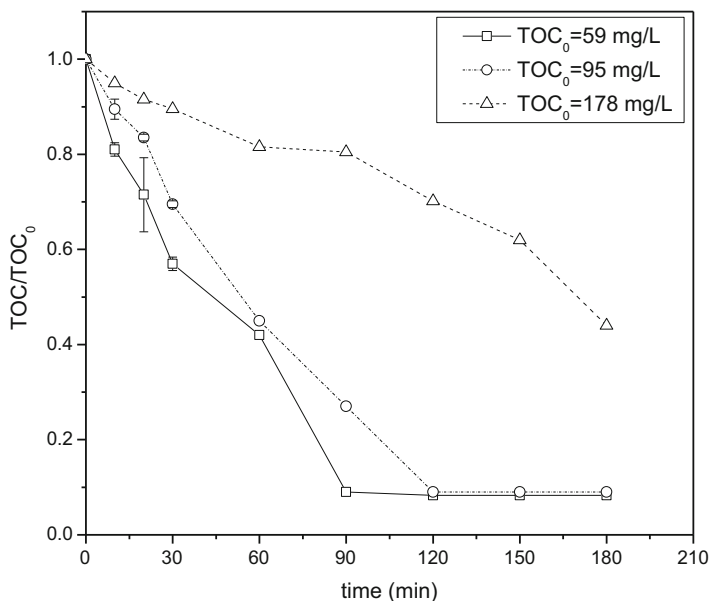
by initial TOC lower than 95 mg/L. Feij Ji et al. also evaluated this variable and reported a similar behavior [38]. At this concentration, it might be that organic molecules absorb less photons in such a way that the photoreduction of Fe(III) is less affected [34, 37, 39, 40]. Thus, the concentration of H_2O_2 dissociation catalyst is higher.

4.5 Effluent Characterization After Photo-Fenton Treatment

In Table 3, a decrease in all parameters after photo-Fenton treatment can be observed. The treatment conditions for such an effluent were as follows: 0.5 g/L of Fe-PILC, stoichiometric concentration of hydrogen peroxide, and pH 2.7. These

Table 3 Effluent characterization after treatment

Parameters	
TOC (mg/L)	78 ± 0.2
COD (mg/L)	56 ± 0.7
pH	2.69 ± 0.01
Conductivity	111 ± 0.7
Temperature	30 °C
Turbidity (NTU)	77 ± 0.7
Dye mg/L (Pt-Co)	0.09 ± 0.007
Concentration (mg/L)	0.006 ± 0.0001
TSS (mg/L)	0

The results are shown as mean $\pm$ standard deviation of two replicate samples

results and those from the acute toxicity study (see Sect. 5) demonstrate that this process can be effectively used to treat wastewater from pharmaceutical industry.

5 Oxidative Stress Determination Prior and Posttreatment Using *Hyalella azteca* as Biomarker

5.1 Procurement, Culturing, and Maintenance of Specimens

Hyalella azteca was collected from its natural habitat in San Miguel de Almaya Lake, municipality of Capulhuac (State of Mexico), and transported to the laboratory under constant aeration in plastic bags. Breeding stock was transported to the laboratory using the water source in which the organisms were reared. Water used for transporting organisms was well oxygenated (90–100% saturated). Upon arrival at the testing laboratory, the organisms were gradually acclimated to the laboratory holding and testing conditions so they would not get stressed. Test organisms were in good health, and the mortality rate for juvenile *Hyalella* did not exceed 20% [47]. The collected organisms were morphologically identified [48]. To eliminate potential differences in sensitivity to contaminants due to acclimation to local conditions or maternal effects, we used organisms from the same clade that had been cultured under the same feeding conditions, temperature, and photoperiod for approximately 4 months (third-generation neonates obtained by sexual reproduction). During culture, specimens were maintained in reconstituted water ($NaHCO_3 = 174$ mg L^{-1}; $MgSO_4 = 120$ mg L^{-1}; $KCl = 8$ mg L^{-1}; and $CaSO_4.2H_2O = 120$ mg L^{-1}; all reagents were obtained from Sigma-Aldrich, St. Louis MO), pH 7.5–8.5, room temperature with constant oxygen (6.4–6.6 mg L^{-1}, O_2), and 12 h/12 h light/dark photoperiod and were fed ground lettuce ad libitum. The estimated number of surviving adults and the production of young in each culture chamber, dates of culture renewals, numbers and age classes of transferred individuals, daily feedings, and water quality measurements were documented.

5.2 Artificial Sediment

The employed artificial sediment was 70% sand (0.2 mm), 20% kaolinite (<0.002 mm), and 10% organic matter (0.2 mm). The organic matter source was lamb compost inactivated by dry heating at 55–60°C for 3 days. The sediment was sterilized with three 15-min autoclave cycles at 121°C and 15-lb pressure, separated by 1-h interval [49, 50].

5.3 Oxidative Stress

Test systems were set up by adding industrial effluent and artificial sediment in a 3:1 ratio to 50-ml polyethylene containers equipped with constant oxygenation and maintained under a 12-h/12-h photoperiod at room temperature. Light intensity adjacent to the surface of the overlying water was 500 lux. The test was conducted at a daily mean temperature (overlying water) of $23 \pm 1°C$. Static systems were used, the medium was not replaced, and no food was provided to specimens during exposure. These systems were added with 1 g of biomass (*Hyalella azteca*), and the exposure time of these organisms to such systems was 96 h. The oxidative stress of an industrial effluent containing paracetamol was determined prior treatment and posttreatment. Once the exposure time was over, 1 g of *Hyalella azteca* was homogenized with phosphate buffer solution. The oxidative stress of the homogenized system was established through lipoperoxidation (LPX) degree by a previously reported method [51]; carbonyl proteins content (CPC) by the modified method of Levine et al. [52]; cumene hydroperoxide (CHP) content by the method of Jiang [53]; activity of the SOD by the method of Misra and Fridovich [54]; and CAT by the method of Radi et al. [55]. This was conducted by triplicate. Also, the protein content was determined [56] in order to normalize the results of the assessed biochemical parameters.

The results in Table 4 show the *Hyalella azteca* oxidative stress biomarkers after 96 h of exposure to treated and untreated effluent samples. It can be observed that the cell oxidation biomarkers were reduced in an interval of 28.6–31.3% with the photo-Fenton treatment. Concomitantly, the antioxidant enzymes were reduced to 28.1–32.51% with the treatment. Based on the summarized results in Table 3, it can be concluded that the treated industrial effluent was less toxic than the untreated one and that, generally speaking, there was a reduction of 30% in all assessed oxidative stress biomarkers.

Regarding oxidative stress, the obtained results in this study are in concordance with those previously reported by Novoa-Luna et al. [57] although at 72 h exposure time. Different studies have pointed out that nonsteroidal anti-inflammatory pharmaceutical compounds like paracetamol are unsteady and photodegraded. Also, it

Table 4 Oxidative stress biomarkers in *Hyalella azteca* prior treatment and posttreatment

Biomarker	Before treatment	After treatment	Biomarker reduction (%)
Lipoperoxidation degree (LPx) [nM de MDA/mg protein]	0.16	0.11	31.3
Hydroperoxides content (CHP) [nM CPH/mg protein)	0.7	0.5	28.6
Carbonyl content in proteins (mM reactive carbonyls/mg proteins)	1.22	0.86	29.5
SOD activity (UI SOD/mg protein)	2.86	1.93	32.5
CAT activity (mM de H_2O_2/mg protein)	32	23	28.1

has been shown that their metabolites are actually more toxic than the parent compounds for aquatic organisms like *Hyalella azteca* [58, 59]. The increase in the oxidative stress biomarkers can be ascribed to the biotransformation of paracetamol (i.e., an NASAID present in the effluent) by the subfamily of cytochrome P450, CYPWC9, that allows the formation of reactive oxygen species (ROS). These ROS can be OH and oxygenated intermediates like the oxy-cytochrome P450 complex [P450 (Fe^{3+}) O^{2*}] as a result of the release of the superoxide anion by reaction decoupling. In both cases, ROS production is increased, which explains the observed increases in LPX and HPC. Also, Gómez-Oliván et al. [60] found similar effects when *H. azteca* was exposed to paracetamol at 770 mg kg^{-1}. This increase may be due to the formation of N-acetyl p benzoquinonimine which is able to bind to cellular membranes.

Thus, the results herein presented show that the photo-Fenton process conducted under pH 8 reduces the toxicity of the pharmaceutical industrial effluent and therefore the oxidative stress biomarkers are considerably reduced. Therefore, it can be concluded that the process is effective at achieving both chemical and biological efficiencies. It is worth pointing out that despite the high mineralization degree achieved under acid pH, the oxidative stress biomarkers were not reduced, thus indicating a high degree of toxicity, probably due to the acid condition of the treated effluent. This implies the need of further addition of chemicals to neutralize the treated effluent and represents a disadvantage of the process that can be overcome by using the proposed catalyst Fe-pillared clay.

6 Conclusions

An industrial effluent was mineralized by photo-Fenton process catalyzed with an iron-pillared clay. The use of this catalyst not only facilitates its recovery (e.g., by magnetism) and reuse after treatment but also allows the use of pH conditions different to those commonly required acidic for a Fenton process. This treatment becomes effective when the effluent has an initial TOC of approximately 200 ppm, otherwise must be diluted. Furthermore, in this process, it is essential to add hydrogen peroxide (H_2O_2) in a stoichiometric ratio with TOC from effluent to be treated; otherwise, other less efficient oxidation mechanisms are promoted. This process leads to a relatively good mineralization degree even without pH modification. A decrease of pH favored Fe leaching and the maximum observed was 4% at a pH 2.7. The results of oxidative stress biomarkers show that the applied process is not only chemically effective but also biologically at pH 8.

References

1. SanJuan-Reyes N, Gómez-Oliván LM, Galar-Martínez M et al (2013) Effluent from an NSAID-manufacturing plant in Mexico induces oxidative stress on Cyprinus carpio. Water Air Soil Poll 224(9):1689
2. Klamerth N, Malato S, Maldonado MI et al (2011) Modified photo-Fenton for degradation of emerging contaminants in municipal wastewater effluents. Catal Today 161:241–246
3. Nunes B, Antunes SC, Santos J, Martins L, Castro BB (2014) Toxic potential of paracetamol to freshwater organisms: a headache to environmental regulators. Ecotoxicol Environ Saf 107:178–185
4. Perez-Moya M, Graells M, Castells G et al (2010) Characterization of the degradation performance of the sulfamethazine antibiotic by photo-Fenton process. Water Res 44:2533–2540
5. Poyatos JM, Muñio MM, Almecija MC et al (2009) Advanced oxidation processes for wastewater treatment: state of the art. Water Air Soil Poll 205:187–204
6. Rozas O, Contreras D, Mondaca MA et al (2010) Experimental design of Fenton and photo-Fenton reactions for the treatment of ampicillin solutions. J Hazard Mater 177:1025–1030
7. Carra I, García Sánchez JL, Casas López JL et al (2014) Phenomenological study and application of the combined influence of iron concentration and irradiance on the Photo-Fenton process to remove micropollutants. Sci Total Environ 478:123–132
8. Cabrera Reina A, Miralles-Cuevas S, Casas López JL et al (2017) Pyrimethanil degradation by photo-Fenton process: influence of iron and irradiance level on treatment cost. Sci Total Environ 605–606:230–237
9. Catalá M, Domínguez-Morueco N, Migens A et al (2015) Elimination of drugs of abuse and their toxicity from natural waters by photo-Fenton treatment. Sci Total Environ 520:198–205
10. Foteinis S, Monteagudo JM, Durán A et al (2018) Environmental sustainability of the solar photo-Fenton process for wastewater treatment and pharmaceuticals mineralization at semi-industrial scale. Sci Total Environ 612:605–612
11. Martin del Campo E, Romero R, Roa G et al (2014) Photo-Fenton oxidation of phenolic compounds catalyzed by iron-PILC. Fuel 138:149–155
12. Xu T, Liu Y, Ge F et al (2013) Application of response surface methodology for optimization of azocarmine B removal by heterogeneous photo-Fenton process using hydroxy-iron–aluminum pillared bentonite. Appl Surf Sci 280:926–932
13. Valverde JL, Amaya R, Romero R et al (2005) Preparation and characterization of Fe-PILCS. Influence of the synthesis parameters. Clays Clay Miner 53(6):613–621
14. Kooli F (2013) Pillared montmorillontes from unusual antiperspirant aqueous solutions: Characterization and catalytic tests. Micropor Mesopor Mat 167:228–236
15. Iurascu B, Siminiceanu I, Vione D et al (2009) Phenol degradation in water through a heterogeneous photo-Fenton process catalyzed by Fe-treated laponite. Water Res 43:1313–1322
16. Benetoli L, De Souza C, Da Silva K, De Souza I, De Santana H, Paesano A, Da Costa A, Zaia C, Zaia D (2007) Amino acid interaction with and adsorption on clays: FT-IR and Mössbauer spectroscopy and X-ray diffractometry investigations. Orig Life Evol Biosph 37:479–493
17. Ericsson T, Wäppling R, Punakivi K (1977) Mössbauer spectroscopy applied to clay and related minerals. Geologiska Föreningen i Stockholm Förhandlingar 99(3):229–244
18. Komlósi A, Kuzmann E, Homonnay Z, Nagy N, Kubuki S, Kónya J (2005) Effect of FeCl$_3$ and acetone on the structure of Na–montmorillonite studied by Mössbauer and XRD measurements. Hyperfine Interact 166:643
19. Kuzmann E, Singh LH, Garg VK, de Oliveira AC, Kovács EM, Molnár AM, Homonnay Z, Kónya P, Nagy NM, Kónya J (2016) Mössbauer study of the effect of rare earth substitution into montmorillonite. Hyperfine Interact 237:2
20. Occelli ML, Stencel JM, Suib SL (1991) Spectroscopic characterization of some iron-containing pillared clays. J Mol Catal 64(2):221–236

21. Schaefer MV, Gorski CA, Scherer MM (2011) Spectroscopic evidence for interfacial Fe(II)−Fe(III) electron transfer in a clay mineral. Environ Sci Technol 45(2):540–545
22. Gibb TC, Greenwood NN (1971) Mössbauer spectroscopy. Chapman and Hall Ltd, London
23. Kuzmann E, Nagy S, Vértes A (2003) Critical review of analytical applications of Mössbauer spectroscopy illustrated by mineralogical and geological examples (IUPAC Technical Report). Pure Appl Chem 75:801–858
24. Parida KM, Mishra T, Das D et al (1999) Thermal transformation of trinuclear Fe(III) acetato complex intercalated montmorillonite. Appl Clay Sci 15(5–6):463–475
25. Bustamante Mamani J, Fernel Gamarra L, Espósito de Souza Brito G (2014) Synthesis and characterization of Fe_3O_4 nanoparticles with perspectives in biomedical applications. Mat Res 17(3):542–549
26. Herojitsingh L, Govindaraja R, Amarendra G et al (2013) Local structure and magnetic properties of cubic iron oxide nanoparticles formed in zeolite as deduced using Mössbauer spectroscopy. Appl Phys Lett 103:193104
27. Johnson CE, Johnson JA, Hah HY et al (2016) Mössbauer studies of stoichiometry of Fe_3O_4: characterization of nanoparticles for biomedical applications. Hyperfine Interact 237:27
28. Ahn T, Kim JH, Yang H-M et al (2012) Formation pathways of magnetite nanoparticles by coprecipitation method. J Phys Chem C 116(10):6069–6076
29. Guyodo Y, Bonville P, Till JL et al (2016) Constraining the origins of the magnetism of lepidocrocite (γ-FeOOH): a Mössbauer and magnetization study. Front Earth Sci 4:28
30. Lozano I, Casillas N, Ponce de León C et al (2017) New insights into the electrochemical formation of magnetite nanoparticles. J Electrochem Soc 164(4):D184–D191
31. Hurtado L, Romero R, Mendoza A, Brewer S, Donkor K, Gómez-Espinosa RM, Natividad R (2019) Paracetamol mineralization by Photo Fenton process catalyzed by a Cu/Fe-PILC under circumneutral pH conditions. J Photochem Photobiol A Chem. 373:162–170
32. Undabeytia T, Galán-Jiménez MC, Gómez-Pantoja E et al (2013) Fe-pillared clay mineral-based formulations of imazaquin for reduced leaching in soil. Appl Clay Sci 80-81:382–389
33. SanJuan-Reyes N, Gomez-Olivan LM, Galar-Martinez M et al (2015) NSAID-manufacturing plant effluent induces geno- and cytotoxicity in common carp (Cyprinus carpio). Sci Total Environ 530-531C:1–10
34. Chen Q, Wu P, Dang Z et al (2010) Iron pillared vermiculite as a heterogeneous photo-Fenton catalyst for photocatalytic degradation of azo dye reactive brilliant orange X-GN. Sep Purif Technol 71:315–323
35. Michael I, Hapeshi E, Michael C et al (2012) Solar photo-Fenton process on the abatement of antibiotics at a pilot scale: degradation kinetics, ecotoxicity and phytotoxicity assessment and removal of antibiotic resistant enterococci. Water Res 46:5621–5634
36. Melero JA, Martinez F, Botas JA et al (2009) Heterogeneous catalytic wet peroxide oxidation systems for the treatment of an industrial pharmaceutical wastewater. Water Res 43:4010–4018
37. Sun J, Feng J, Shi S et al (2012) Degradation of the antibiotic sulfamonomethoxine sodium in aqueous solution by photo-Fenton oxidation. Chin Sci Bull 57:558–564
38. Ji F, Li C, Zhang J et al (2011) Heterogeneous photo-Fenton decolorization of methylene blue over LiFe(WO_4)_2 catalyst. J Hazard Mater 186:1979–1984
39. Pariente M, Martinez F, Melero J et al (2008) Heterogeneous photo-Fenton oxidation of benzoic acid in water: effect of operating conditions, reaction by-products and coupling with biological treatment. Appl Catal B-Environ 85:24–32
40. Ayodele OB, Lim JK, Hameed BH (2012) Pillared montmorillonite supported ferric oxalate as heterogeneous photo-Fenton catalyst for degradation of amoxicillin. Appl Catal A-Gen 413-414:301–309
41. Herney-Ramirez J, Vicente MA, Madeira LM (2010) Heterogeneous photo-Fenton oxidation with pillared clay-based catalysts for wastewater treatment: a review. Appl Catal B-Environ 98:10–26
42. De León MA, Castiglioni J, Bussi J et al (2008) Catalytic activity of an iron-pillared montmorillonitic clay mineral in heterogeneous photo-Fenton process. Catal Today 133–135:600–605

43. Najjar W, Azabou S, Sayadi S et al (2007) Catalytic wet peroxide photo-oxidation of phenolic olive oil mill wastewater contaminants. Appl Catal B-Environ 74:11–18

44. Sadok Letaïef BC, Aranda P, Martín-Luego MA et al (2003) Fe-containing pillared clays as catalysts for phenol hydroxylation. Appl Clay Sci 22:263–277

45. Bobu M, Yediler A, Siminiceanu I et al (2008) Degradation studies of ciprofloxacin on a pillared iron catalyst. Appl Catal B-Environ 83:15–23

46. González-Bahamón LF, Mazille F, Benítez LN et al (2011) Photo-Fenton degradation of resorcinol mediated by catalysts based on iron species supported on polymers. J Photoch Photobio A 217:201–206

47. Agency, U.-U. S. E. P (2000) Methods for measuring the toxicity and bioaccumulation of sediment-associated contaminants with freshwater invertebrates. Page 192 Report EPA 600/R-99/064. Prepared by the Office of Research and Development, Mid-Continent Ecology Division, USEPA, Duluth, Minnesota, and the Office of Science and Technology, Office of Water, USEPA, Washington, DC

48. Pennak RV (1978) Freshwater invertebrates of the United Sates. 2nd edn. Wiley, New York

49. (OECD), O. f. t. E. C. a. D (1984) Guidelines for the testing of chemicals. Guideline 207: earthworm acute toxicity test OECD publications service, Paris, p 9

50. (SETAC), S. o. E. T. a. C.-E (1993) Guidance document on sediment toxicity test and bioassays for freshwater and marine environments. Workshop on Sediment Toxicity Assessment. SETAC, Amsterdam

51. Büege JA, Aust SD (1978) Microsomal lipid peroxidation. Method Enzymol 52:302–310

52. Levine RL, Williams JA, Stadtman ER et al (1994) Carbonyl assays for determination of oxidatively modified proteins. Method Enzymol 233:346–357

53. Jiang ZY, Hunt JV, Wolff SP (1992) Ferrous ion oxidation in the presence of xylenol orange for detection of lipid hydroperoxide in low density lipoprotein. Anal Biochem 202:384–389

54. Misra HP, Fridovich I (1972) The role of superoxide anion in the autoxidation of epinephrine and a simple assay for superoxide dismutase. J Biol Chem 247:3170–3175

55. Radi R, Turrens JF, Chang LY et al (1991) Detection of catalase in rat heart mitochondria. J Biol Chem 266:22028–22034

56. Bradford M (1976) A rapid and sensitive method for the quantitation of microorganism quantities of protein utilizing the principle of protein dye binding. Anal Biochem 72:248–254

57. Novoa-Luna KA, Romero-Romero R, Natividad-Rangel R et al (2016) Oxidative stress induced in Hyalella azteca by an effluent from a NSAID-manufacturing plant in Mexico. Ecotoxicology 25(7):1288–1304

58. Araujo L, Villa N, Camargo N et al (2011) Persistence of gemfibrozil, naproxen and mefenamic acid in natural waters. Environ Chem Lett 9:13–18

59. Borgmann U, Bennie DT, Ball AL et al (2007) Effect of a mixture of seven pharmaceuticals on Hyalella azteca over multiple generations. Chemosphere 66:1278–1283

60. Gómez-Oliván LM, Neri-Cruz N, Galar-Martínez M et al (2012) Assessing the oxidative stress induced by paracetamol spiked in artificial sediment on Hyalella azteca. Water Air Soil Pollut 223:5097–5104